Formation of turbulent structures and the link to fluctuation driven sheared flows

T. Windisch[1], **O. Grulke**[1,2], **V. Naulin**[3], **T. Klinger**[1,2]

[1] Max-Planck-Institute for Plasma Physics, EURATOM Association, D-17491 Greifswald, Germany
[2] Ernst-Moritz-Arndt University, D-17489 Greifswald, Germany
[3] Risø DTU, Technical University of Denmark

E-mail: thomas.windisch@ipp.mpg.de

Abstract.
The formation of turbulent structures in weakly-developed drift wave turbulence is investigated using experimental data obtained in a linear laboratory device. The findings are compared with fully nonlinear numerical simulation results. The formation of structures occurs in a region, in which the divergence of the Reynolds stress, which is one term in the momentum balance, has a maximum. The generation of a time-averaged shear layer is not observed, but for transient events the shearing rate can get sufficiently strong to decorrelate the fluctuations. This happens when the energy flow into the shear flow is largely positive.

PACS numbers: 52.35.Kt,52.35.Ra,52.35.Mw

Keywords: intermittency, $E \times B$-shear, turbulence, drift-waves, transport

1. Introduction

Experimental observations [1, 2] and numerical simulations [3] clearly demonstrate that the turbulent particle flux in the region of open magnetic flux surfaces of fusion devices is dominated by radially propagating coherent turbulent structures, so called blobs. These structures cause an intermittent character of pressure fluctuations, characterized by sporadic large amplitude bursts. They emerge from broad-band turbulence in the plasma edge and their dynamics in the scrape-off layer (SOL) region is determined by the balance of the interchange drive, which relies on the curvature of the magnetic field [4], parallel losses along the magnetic field and perpendicular currents, e.g. due to ion polarization drifts or ion viscosity, in the region of magnetic shear (e.g. X-point region) [5] . While the formation of these structure is difficult to study in fusion devices due to limitations in the available diagnostics, laboratory devices like Torpex have shown that these structures can be sheared off from interchange wave crests due to their self-consistent $E \times B$-velocity shear [6]. Similar intermittent fluctuations related to radially propagating three-dimensional structures are also observed in linear laboratory devices with straight magnetic field geometry [7, 8]. In this case the interchange drive is absent and thought to be replaced by centrifugal [9] or neutral wind forces [10].

A recent issue of blob dynamics is the associated transport of momentum from the plasma edge into the scrape-off layer (SOL) [11, 5], which might explain the spontaneous toroidal rotation observed in fusion devices [12]. A similar mechanism has been suggested to explain the formation of isolated blobs [13]. The mechanism is closely connected to the formation of zonal flows, which are driven by the divergence of turbulent Reynolds stress $< \tilde{v}_x \tilde{v}_y >$ ($< \cdot >$ denotes the zonal average). It has been shown that in the limit of vanishing zonal flow shear damping rate, where the Reynolds stress contribution to the poloidal momentum is balanced by the passive radial convection, the convective transport is dominated by blobs [13]. In contrast, if the zonal flow shear damping rate is large the convective transport is determined by radial streamers.

In the present paper the relation between sheared flows and the formation of coherent turbulent structures is analyzed in a linearly laboratory device. In Sec. 2 the main experimental findings are summarized. In Sec. 3 the experimental observations are compared to numerical simulation results using the three-dimensional CYTO code [14] and influence of sheared flows on the fluctuation dynamics is investigated in detail. Finally, the results are summarized in Sec. 4.

2. Experimental observations

The experiments have been performed in the linearly magnetized helicon VINETA device [15]. For a detailed description of the experimental setup and operational parameters the reader is referred to [16]. Radial profiles of time-averaged plasma density n and its corresponding *rms*-fluctuation level $\tilde{n}$ as measured with Langmuir probes are shown in Fig. 1a. The peak density is $n \approx 6 \times 10^{18}\,\mathrm{m}^{-3}$ and the profile has almost a Gaussian shape. The electron temperature (not shown here) is 2.5 eV in the plasma centre and decreases to 1 eV in the edge ($r > 100\,\mathrm{mm}$). The *rms*-fluctuation amplitude peaks close to the region of the maximum density gradient region with $\tilde{n} \approx 10 - 15\%$. Detailed investigations have shown that the fluctuation dynamics in VINETA is dominated by the drift-wave instability [17], which is driven by the

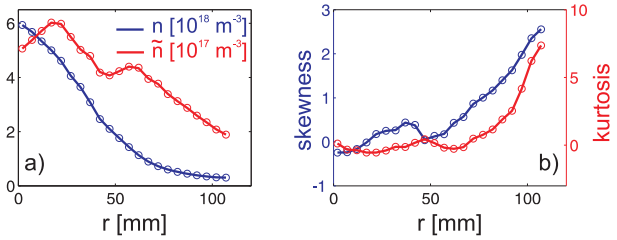

Figure 1. a) Time-averaged radial plasma density profile and corresponding *rms*-fluctuation level. b) Radial evolution of skewness and kurtosis of density fluctuations.

radial density gradient. With the magnetic field as control parameter the system can be driven from single coherent drift modes to a weakly developed turbulent regime, which is characterized by non-linearly interacting modes [18]. The character of density fluctuations changes significantly across the radial plasma density profile. This can be quantified by the moments of the probability density function (PDF), i.e. skewness and kurtosis, which are shown in Fig. 1b. For $r < 55\,\mathrm{mm}$ both moments are close to zero, which indicates nearly Gaussian distributed fluctuations. For $r > 55\,\mathrm{mm}$ the moments increase considerably, which is caused by intermittent positive large-amplitude bursts. It has been demonstrated that intermittent bursts are related to radially propagating turbulent structures, which peel-off from a quasi-coherent $m = 1$ drift mode (m being the azimuthal modenumber) [16]. The peel-off region here is located at $r \approx 55\,\mathrm{mm}$. It is worthwhile to note that the skewness is negative for $r < 20\,\mathrm{mm}$, which indicates a dominant contribution of negative density bursts (so-called holes), which are also observed in the plasma edge region of fusion devices [19].

The transition from the $m = 1$ drift mode to isolated turbulent structures is accompanied by a strong shear of the azimuthal phase velocity v_{ph} (Fig.2a). It has been measured using two azimuthally separated probes. The time delay of the maximum cross-correlation then yields an estimate of v_{ph}. A positive velocity v_{ph} corresponds to a propagation in electron diamagnetic drift direction and a negative velocity corresponds to a propagation in direction of the background $E \times B$-drift [16]. Since the sudden change of the phase velocity in the transition region at

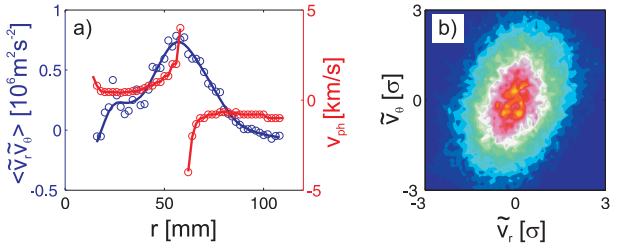

Figure 2. a) Radial profile of the time-averaged Reynolds stress (blue) and phase velocity v_{ph} (red). b) Joint probability density function (PDF) of fluctuating radial and azimuthal velocities (normalized to the standard deviation σ).

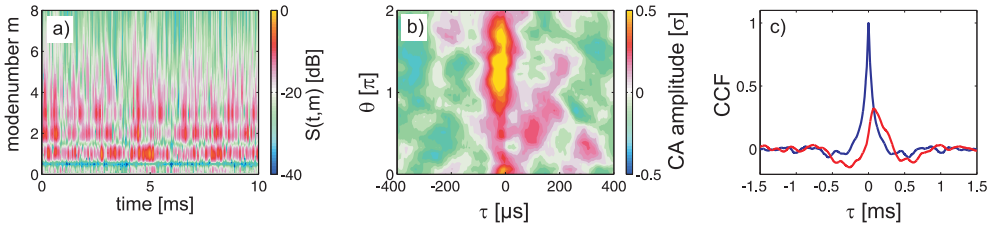

Figure 3. a) Temporally resolved modenumber spectrum of potential fluctuations at $r = 52\,\mathrm{mm}$. b) Conditionally averaged azimuthal potential fluctuations (see text for details). c) Auto-correlation function of the azimuthally averaged Reynolds stress $< \tilde{v}_r\tilde{v}_\theta >$ (blue) and cross-correlation between the $< \tilde{v}_r\tilde{v}_\theta >$ and $\tilde{\phi}_{m=0}$ (red).

$r \approx 50\,\mathrm{mm}$ cannot be explained by time-averaged first order fluid drifts, which are determined by the density and potential profile [16], the turbulent Reynolds stress is considered as momentum source. The radial divergence of the Reynolds stress is directly associated with the generation of a mean azimuthal flow $< v_\theta >$ [20], $\partial_t < v_\theta >= -\partial_r < \tilde{v}_r\tilde{v}_\theta >$, where $< v_\theta >= \partial_r < \tilde{\phi} >= \partial_r\tilde{\phi}_{m=0}$. Here $\tilde{\phi}_{m=0}$ denotes the $m = 0$ mode of the fluctuating potential. To obtain a radial profile of the Reynolds stress the azimuthal average is replaced by the time-average $< \tilde{v}_r\tilde{v}_\theta >_t$. The latter is shown in Fig. 2a as blue line. It is measured using an array of four Langmuir probes which record floating potential fluctuations at two different radial and two different azimuthal positions with a spacing of 8 mm in both directions. This allows to estimate the corresponding electric fields and the fluctuating electric drift velocities $\tilde{v}_r$ and $\tilde{v}_\theta$. Previous measurements using emissive probes have shown that temperature fluctuations are small such that floating potential fluctuations can be taken as a measure of plasma potential fluctuations [21]. As can be seen in Fig. 2a the term $< \tilde{v}_r\tilde{v}_\theta >_t$ has a positive maximum at $r = 55\,\mathrm{mm}$ that corresponds to the transition region. The Reynolds stress demands a certain correlation between the radial and azimuthal velocity fluctuations. This can be observed in the joint PDF of the velocity fluctuations at $r = 55\,\mathrm{mm}$, which is shown is Fig.2b. Due to the tilted PDF positive radial velocities directed radially outwards are in phase with azimuthal velocities and lead to a positive Reynolds stress, as observed in Fig. 2a. Similar results have also been observed in the CSDX device [22].

In order to investigate the relation between the Reynolds stress and $\tilde{\phi}_{m=0}$ in more detail the potential fluctuations have been measured using an azimuthal probe array consisting of 64 Langmuir probes with alternating radial positions ($r = 52\,\mathrm{mm}$ and $r = 60\,\mathrm{mm}$). This allows to measure the azimuthally averaged Reynolds stress in the transition region. The temporally resolved modenumber power spectrum of potential fluctuations at $r = 52\,\mathrm{mm}$ is shown in Fig. 3a. The main spectral energy is broadly distributed between the larger spatial scales with $m \leq 6$ but peaks at $m = 1$. On average the energy of the $m = 0$ is much smaller than the contribution of the higher modenumbers but at certain time instants it becomes comparable. To ensure that the estimated energy of the $m = 0$ mode is not an artefact of the spectral analysis (spectral leakage), the conditional average (CA) technique [23] has been used. The reference condition was set to the spectral amplitude of the $m = 0$ mode with an amplitude condition of $p = 1\sigma$ (σ denotes the standard deviation) and the CA amplitude has been

calculated for all 32 Langmuir probes at this radius. The result is shown in Fig. 3b. If the amplitude of $\tilde{\phi}_{m=0}$ is high the potential fluctuations display the dominance of an $m = 0$ mode, i.e. the fluctuating azimuthal mean is rather caused by a zonal structure than by a large amplitude perturbation with a smaller scale. Using the azimuthal probe array the correlation between the Reynolds stress and $\tilde{\phi}_{m=0}$ can directly be estimated. The resulting cross-correlation amplitude is shown in Fig. 3c (red line) together with the auto-correlation function of the Reynolds stress (as blue line). The frequency averaged cross-correlation has a maximum amplitude of 0.3, which clearly exceeds the statistical noise level.

The results suggest that in the transition region a fluctuating $m = 0$ potential perturbation exists, which is driven by the turbulent Reynolds stress. On time-average the contribution of $\tilde{\phi}_{m=0}$ to the fluctuation spectrum is only small. But at particular time instants this contribution can become dominant. This happens when the energetic drive of the mean flow $R \sim < \tilde{v}_r \tilde{v}_\theta > < \Omega > = < \tilde{v}_r \tilde{v}_\theta > \partial_r < v_\theta >$ has a positive amplitude (here $\Omega = \nabla_\perp^2 \phi$ denotes the vorticity) [24, 25]. This means if the turbulent structures are tilted by a seed shear flow with a shear rate $\partial_r < v_\theta >$ and the Reynolds stress has the same orientation, energy is transferred from the turbulent fluctuations into the mean flow, which amplifies the latter [26]. In the experiment, the temporal evolution of the shear rate, caused by a nonlinearly driven $m = 0$ potential perturbation, cannot be analyzed due to limitations of the available diagnostics. This issue and the relation between $\tilde{\phi}_{m=0}$ and the formation of turbulent structures in the transition region is analyzed in more detail in the next section using numerical simulation results.

3. Numerical simulation results

The numerical simulation results presented here are done with the CYTO code [14]. The code solves the two-fluid equations in a three-dimensional cylindrical geometry with sheath boundary conditions and an axially localized Gaussian density source profile. A specific feature of the code is the global character, i.e. a Reynolds decomposition into mean and fluctuating quantities is not applied. This is especially important in the plasma edge, where the amplitude of intermittent density burst clearly exceed the time-averaged density. The input parameters of the code are similar to the experimental situation presented in SEC.2. In a similar representation

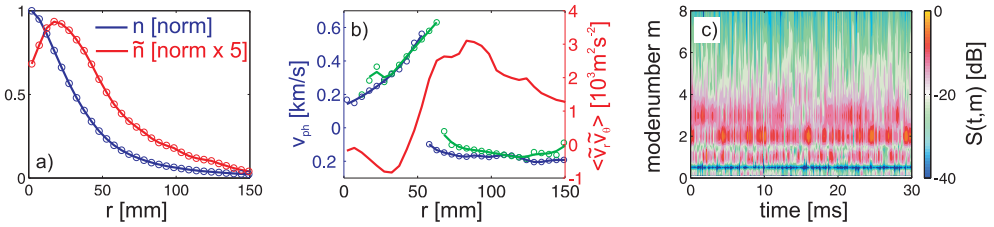

Figure 4. a) Normalized radial profiles of plasma density and corresponding *rms*-fluctuation level. b) Radial profile of the time-averaged Reynolds stress (red) and phase velocity v_{ph} (blue,green) (see text for details). c) Temporal evolution of the azimuthal modenumber spectrum of potential fluctuations at $r = 68$ mm.

as for the experimental results the normalized radial plasma density profile is shown in Fig.4a, together with the corresponding *rms*-fluctuation level. The density profile is mainly determined by the Gaussian source profile. In agreement to the experimental situation the *rms*-fluctuation amplitude peaks in the maximum density gradient region with an amplitude of $\tilde{n}_{rms} \approx 20\%$. The spatiotemporal evolution of the fluctuations across the plasma cross-section has been analyzed in detail in Ref. [16]. Similar to the experimental situation the dynamics in the maximum density gradient region is dominated by drift waves with low modenumbers ($m = 1, 2$). For larger radii coherent turbulent structures are observed, which propagate radially outwards and cause an intermittent character of the density fluctuations in the plasma edge. Also in this case the formation of the structures can be explained as a peel-off process from positive wave crests associated with drift modes in a narrow radial transition region. This transition region can be observed in Fig. 4b, in which two different estimates of the radial evolution of the phase velocity v_{ph} are shown. The first estimate (blue line) is based on the dominant contribution in the frequency-modenumber spectrum (m, f)-spectrum computed at each radial position and the second estimate (green line) uses the cross-correlation technique as in the experimental case. Both estimates agree well but in the transition region at $r \approx 60\,\mathrm{mm}$ small deviations are observed, which are caused by the local approximation of the cross-correlation technique. For a close comparison with the experimental situation the time averaged Reynolds stress profile is also shown in Fig. 4b (red line), which demonstrates that also here the transition region corresponds to a positive maximum of the Reynolds stress. The temporally resolved modenumber power spectrum of potential fluctuations at $r = 68\,\mathrm{mm}$ is shown in Fig. 4c. It is dominated by large scale fluctuations with $m \leq 4$ but sporadic contributions of $\tilde{\phi}_{m=0}$ are clearly observed. Before analyzing the energy transfer to the mean flow in detail the different contributions to the momentum flux are considered. The electrostatic momentum flux can be written as [27]

$$\Pi = < n >< \tilde{v}_r \tilde{v}_\theta > + < v_\theta >< n\tilde{v}_r > + < \tilde{n}\tilde{v}_\theta \tilde{v}_r >,$$

where the terms of the rhs are the Reynolds stress contribution, passive convection, and non-linear flux. Time-series of these three contributions averaged over the azimuthal cross-section are shown in Fig. 5a. On time-average the Reynolds stress has a positive mean and dominates the momentum flux. But it is partly balanced by the

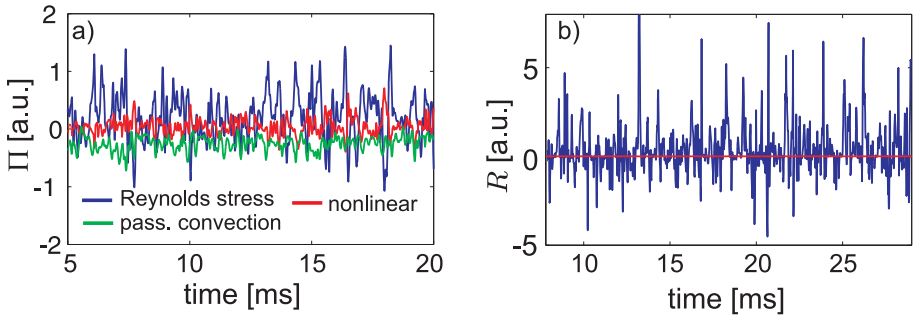

Figure 5. a) Time-series of the contributions to the momentum flux (averaged over the azimuthal cross-section). b) Time-series of the energy transfer rate R.

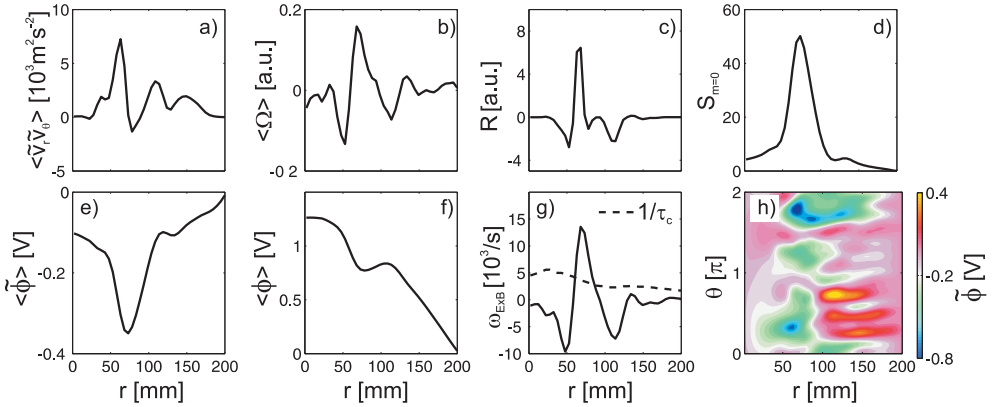

Figure 6. Radial profiles of Reynolds stress $< \tilde{v}_r \tilde{v}_\theta >$ (a), vorticity $< \Omega >$ (b), energetic drive R (c), spectral energy of $\tilde{\phi}_{m=0}$ (d), amplitude of $\tilde{\phi}_{m=0}$ (e), amplitude of $< \phi >$ (f), and shearing rate $\omega_{E\times B}$ (g) at a single time instant. The corresponding two-dimensional potential snapshot is shown in (h).

passive convection, which has a negative mean. The non-linear term has the same magnitude as the passive convection. The temporal evolution of the energy transfer rate $R \sim < \tilde{v}_r \tilde{v}_\theta >< \Omega >$ in the transition region ($r = 68\,\mathrm{mm}$) is shown in Fig. 5b. The transfer rate has a positive mean, which means that on average energy is transferred from the fluctuations to the mean flow. The time series also shows that the transfer rate is governed by sporadic large amplitude events. The complex situation during such a strong positive transfer event is shown in Fig. 6. At $r \approx 60\,\mathrm{mm}$ both $< \tilde{v}_r \tilde{v}_\theta >$ and $< \tilde{\Omega} >$ have a positive peak, which in turn leads to a pronounced positive amplitude of the energetic drive R (Fig. 6c). The radial evolution of the spectral energy of $\tilde{\phi}_{m=0}$ (Fig. 6d) also peaks at this position. At this particular time instant the contribution of higher modes is negligibly small. The amplitude of the $\tilde{\phi}_{m=0}$ mode and $< \phi >$ are shown in Fig. 6e-f. Compared to the time-averaged potential profile (cf. Fig. 4)

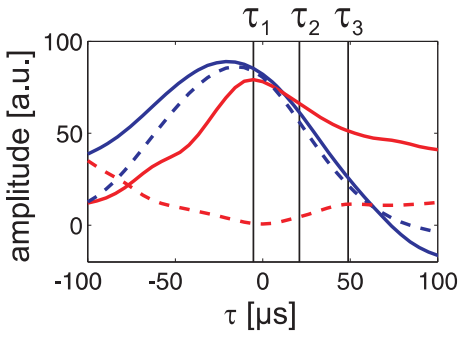

Figure 7. Reference signals for the conditional averaging analysis using two reference signals: density (blue) and $\tilde{\phi}_{m=0}$ (red). The solid (dashed) lines indicate the case for a large (small) $\tilde{\phi}_{m=0}$ amplitude (see text for details).

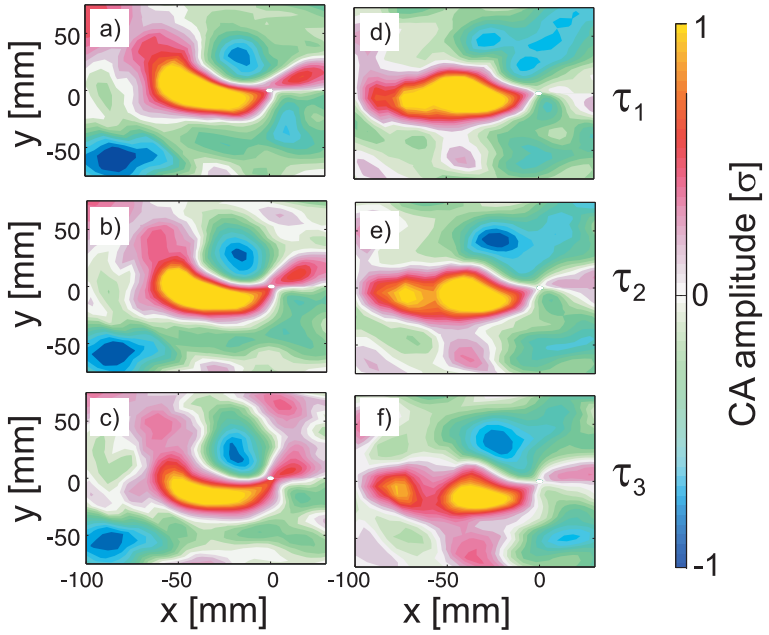

Figure 8. Conditionally averaged density fluctuations using two reference conditions for three time instants $\tau_{1,2,3}$, which are indicated in Fig. 7 (see text for details). The cases (a-c) corresponds to a negligible contribution of $\tilde{\phi}_{m=0}$ and (d-f) to a significant contribution of $\tilde{\phi}_{m=0}$ to the fluctuation spectrum.

a pronounced dip at $r = 75$mm is observed. As a consequence the shearing rate $\omega_{E\times B} = \partial_r < v_\theta >$ increases significantly and exceeds the inverse autocorrelation time of the fluctuations (indicated in Fig. 6g as dashed line). A two-dimensional snapshot of the fluctuating potential is shown in Fig. 6h. The dominance of the $m = 0$ contribution to the fluctuation spectrum is clearly observed at $r = 60$ mm but higher modes do also contribute. In summary, if the energetic drive R amplifies the mean flow the shearing rate becomes sufficiently strong to decorrelate the turbulent fluctuations. A statistical analysis of the modification of density fluctuations during such a strong $\tilde{\phi}_{m=0}$ contribution is rather complicated because both quantities are not well correlated. However, evidence for an influence of the fluctuation-driven shear flow on the spatiotemporal evolution of density perturbations can be obtained by the local conditional averaging technique using two reference conditions: The first reference condition is set to density fluctuations at $r = 42$ mm with an amplitude threshold of 2σ. The second reference condition is set to $\tilde{\phi}_{m=0}$ at $r = 68$ mm. Here two different amplitude thresholds are chosen: In the first case $\tilde{\phi}_{m=0}$ dominates the fluctuation spectrum and in the second case the contribution of $\tilde{\phi}_{m=0}$ to the fluctuation spectrum is negligible small. The reference signals for both cases are shown in Fig. 7. The blue lines indicate the density reference signal and the red lines indicate the $\tilde{\phi}_{m=0}$ reference signal. For the two cases the density reference signals are almost identical. For the time instants $\tau_{1,2,3}$ indicated in Fig. 7 the conditionally averaged density fluctuations are shown in Fig. 8 for the case of a negligible small (Fig. 8a-c) and large (Fig. 8d-f)

amplitude of $\tilde{\phi}_{m=0}$. In both cases a large positive $m = 2$ drift mode perturbation is observed. A careful analysis reveals that in the case of a significant contribution of $\tilde{\phi}_{m=0}$ a small structure starts to radially peel off the positive drift mode perturbation. This is not observed in the case with negligible small amplitude of $\tilde{\phi}_{m=0}$. It should be mentioned here that the number of events which contribute to the CA ensemble average is only 20, which forbids to draw detailed conclusions.

4. Summary

In the present paper the relation between the Reynolds stress and the formation of turbulent structures has been investigated by means of experimental data obtained in a linearly magnetized laboratory device and numerical simulations results. In both cases clear evidence has been found that the turbulent Reynolds stress drives a fluctuating $m = 0$ potential perturbation $\tilde{\phi}_{m=0}$. The radial profile of the Reynolds stress peaks in a region, in which turbulent structures peel-off from quasi-coherent drift modes [16]. Although the time-averaged amplitude of $\tilde{\phi}_{m=0}$ is much smaller compared to the contribution of the fluctuations with larger modenumbers (smaller scales), it can become dominant if the energetic transfer R rate gets sufficiently large. In this case a strong increase of the shear rate is observed, which can decorrelate the turbulent fluctuations. The conditional averaging result presented in Sec. 3 gives a strong indication that the peel-off process of the turbulent structures is related to this transient increase of $\tilde{\phi}_{m=0}$.

References

[1] Zweben S J, Maqueda R J, Stotler D P, Keese A, Boedo J, Bush C E, Kaye S M, LeBlanc B, Lowrance J L, Mastrocola V J, Maingi R, Nishino N, Renda G, Swain D W, Wilgen J B and the NSTX Team 2004 *Nucl. Fusion* **44** 134–153

[2] Terry J L, Zweben S J, Hallatschek K, LaBombard B, Maqueda R J, Bai B, Boswell C J, Greenwald M, Kopon D, Nevins W M, Pitcher C S, Rogers B N, Stotler D P and Xu X Q 2003 *Phys. Plasmas* **10** 1739–1747

[3] Garcia O E, Naulin V, Nielsen A H and Rasmussen J J 2004 *Phys. Rev. Lett.* **92** 165003

[4] Krasheninnikov S I 2001 *Phys. Lett. A* **283** 368–370

[5] Myra J R, Russell D A and D'lppolito D A 2008 *Phys. Plasmas* **15** 032304

[6] Furno I, Labit B, Podesta M, Fasoli A, Muller S H, Poli F M, Ricci P, Theiler C, Brunner S, Diallo A and Graves J 2008 *Phys. Rev. Lett.* **100** 055004

[7] Windisch T, Grulke O and Klinger T 2006 *Phys. Plasmas* **13** 122303

[8] Carter T A 2006 *Phys. Plasmas* **13** 010701

[9] Popovich P, Umansky M V, Carter T A and Friedman B 2010 *Phys. Plasmas* **17** 102107

[10] Krasheninnikov S I and Smolyakov A I 2003 *Phys. Plasmas* **10** 3020–3021

[11] Labit B Labit B, Theiler C, Fasoli A, Furno I and Ricci P 2011 *Phys. Plasmas* **18** 032308

[12] Coppi B 2002 *Nucl. Fusion* **42** 1–4 ISSN 0029-5515

[13] Russell D A, Myra J R and D'Ippolito D A 2009 *Phys. Plasmas* **16** 122304

[14] Naulin V, Windisch T and Grulke O 2008 *Phys. Plasmas* **15** 012307

[15] Franck C M, Grulke O and Klinger T 2002 *Phys. Plasmas* **9** 3254–3258

[16] Windisch T, Grulke O, Naulin V and Klinger T 2011 *Plasma Phys. Controlled Fusion* **53** 085001

[17] Schröder C, Grulke O, Klinger T and Naulin V 2004 *Phys. Plasmas* **11** 4249–4253

[18] Brochard F, Windisch T, Grulke O and Klinger T 2006 *Phys. Plasmas* **13** 122305

[19] Nold B, Conway G, Happel T, Mu uml ller H, Ramisch M, Rohde V and Stroth U 2010 *Plasma Phys. Controlled Fusion* **52** 065005

[20] Diamond P and Kim Y 1991 *Phys. Fluids B* **3** 1626–1633

[21] Schrittwieser R, Ionita C, Balan P, Gstrein R, Grulke O, Windisch T, Brandt C, Klinger T, Madani R, Amarandei G and Sarma A K 2008 *Rev. Sci. Instrum.* **79** 083508

[22] Yan Z, Yu J H, Holland C, Xu M, Muller S H and Tynan G R 2008 *Phys. Plasmas* **15** 092309

[23] Adrian R J 1979 *Phys. Fluids* **22** 2065–2070

[24] Naulin V, Kendl A, Garcia O E, Nielsen A H and Rasmussen J J 2005 *Phys. Plasmas* **12** 052515
[25] Scott B D 2005 *New J. Phys* **7** 92
[26] Manz P, Ramisch M and Stroth U 2009 *Phys. Rev. Lett.* **103** 165004
[27] Diamond P H, McDevitt C J, Gurcan O D, Hahm T S, Wang W X, Yoon E S, Holod I, Lin Z, Naulin V and Singh R 2009 *Nucl. Fusion* **49** 045002